Supporting Information

3D hierarchical Nitrogen-doped carbon nanoflower derived from chitosan for electrocatalytic oxygen reduction and high performance lithium-sulfur batteries

Daying Guo[a], Huifang Wei[a], Xi'an Chen[a]*, Menglan Liu[a], Feng Ding[a], Zhi Yang[a], Yun Yang[a], Shun Wang[a], Keqin Yang[a], Shaoming Huang[a,b]*

[a]Key Laboratory of Carbon Materials of Zhejiang Province, College of Chemistry and Materials Engineering, Wenzhou University, Wenzhou 325035, P.R. China.

[b]School of Materials and Energy, Guangdong University of Technology, Guangzhou, Guangdong 510006 P.R. China.

E-mail: xianchen@wzu.edu.cn (Xi'an Chen), smhuang@wzu.edu.cn (Shaoming Huang)

Electrochemical measurements

ORR electrode The working electrode was first polished by 50 nm Al_2O_3 powder, and then was treated with deionized water and ethanol respectively by ultrasonic 10 s. The products 2 mg NCNF was dispersed by ultrasonically into 500 μL of ethanol (Aladdin Chemical Reagent Co., Ltd). Then 10 μL of the resulting suspension were dropped onto the GC surface, 5 μL 0.5 wt% Nafion was dropped into the surface of NCNF in semi-dry state, then continued to dry at room temperature for 4 h for electrochemical tests. The electrolyte was 0.1M KOH solution, and test process to maintain 20 °C. In the process of testing the electrolyte must advance through the oxygen and nitrogen 30 min. For comparison, a commercially available Pt/C catalyst (20 wt% Pt) modified GC working electrode was prepared in the same method. CV (cyclic voltammetry), LSV (liner sweep voltammetry), and RRDE (rotating ring disk electrode) measurements were employed on the CHI 660E electrochemical workstation (Shanghai Chenhua) with a Pine Modulated Speed Rotator (PINE

Co.,Ltd). Electrochemical tests were performed at room temperature in 0.1 M KOH solutions by a three-electrode cell, in which platinum-wire was used as counter electrode and Ag//AgCl (in 3M KCl solution) as reference electrode, which were purged with high purity nitrogen or oxygen for at least 30 min prior to each measurement. The measured potentials *vs.* Ag//AgCl (in 3M KCl solution) were referred to the reversible hydrogen electrode (RHE) scale according to the Nernst equation:

$$E_{RHE} = E_{Ag/AgCl} + 0.059pH + E°_{Ag/AgCl}$$

where $E_{Ag/AgCl}$ is the experimentally measured potential *vs* Ag/AgCl reference and $E°_{Ag/AgCl}$ = 0.21 V at 20 °C. The values of potential provided along the text are referenced against RHE unless otherwise stated. CV was performed from -0.2 to 1.4 V *vs* RHE in O_2- and N_2-saturated 0.1 M KOH electrolytes, with a sweep rate of 30 mV s^{-1}. RDE LSV measurements were conducted from 1 to 0 V *vs* RHE in O_2-saturated 0.1 M KOH electrolytes at a scan rate of 10 mV s^{-1} under disk rotation rates of 400, 425, 900, 1225, 1600, 2025, 3025 and 3600 rpm. The working electrode was a 5.0 mm diameter GC rotating disk electrode. The apparent number of electrons transferred during ORR on the carbon catalysts was determined by the Koutechy−Levich equation given by

$$\frac{1}{J} = \frac{1}{J_L} + \frac{1}{J_K} = \frac{1}{B\omega^{1/2}} + \frac{1}{J_K}$$

$$B = 0.62\, nFC_0 (D_0)^{2/3} \nu^{1/6}$$

where J is the measured current density, J_K is the kinetic current density, J_L is the diffusion-limited current density, ω is the electrode rotation rate, F is the Faraday constant (96500 C mol^{-1}), C_0 is the bulk concentration of O_2 (1.2×10^{-3} mol L^{-1} 0.1 M KOH solution), D_0 is the diffusion coefficient of O_2 (1.9×10^{-5} cm^2 s^{-1} for 0.1 M KOH solution), and ν is the kinetic viscosity of the electrolyte (0.1 M KOH solution)[1,2].

For the RRDE tests, the disk potential was scanned at 10 mV s^{-1} and was fixed at 1600rpm, while the ring potential was set to be 0.5 V *vs* RHE in order to H_2O_2 produced[2, 3]. The working electrode was a 5 mm glassy carbon disk electrode and a

Pt ring electrode. The H_2O_2 collection efficiency at the ring (N = 0.249) was provided by the manufacturer. The following equations were used to calculate n (electrons transferred number) and % H_2O_2 (percent content of hydrogen peroxide)

$$n=\frac{4|I_D|}{|I_D|+(I_R/N)}$$

$$\%H_2O_2=100\times\frac{2I_R/N}{|I_D|+(I_R/N)}$$

where n is the electron-transfer number, I_D is the disk current, I_R is the ring current, and N is the H_2O_2 collection coefficient.

The catalytic stability of the material was conducted by i-t curve in the voltage 0.68V, under the oxygen atmosphere in 0.1 M KOH solution.

Lithium-Sulfur Cathode

NCNF/S composites was mixed with acetylene black and polyvinylidene fluoride (PVDF) at a mass ratio of 80:10:10 with N -methyl pyrrolidone (NMP) as a dispersant. Electrode paste was coated on aluminum foil with different specifications and was cutting into a film disk of 14 mm in diameter. The as-obtained film disk was dried in a vacuum oven at 60 °C for 12 h. CR2025-type coin cells were fabricated by sandwiching a porous polypropylene separator between the film disk of NCNF/S and a lithium metal foil in a high-purity argon filled glove box. 1wt% anhydrous lithium nitrate (analytical grade) and 1 M $LiN(CF_3SO_2)_2$(LiTFSI) in a mixed solvent of 1,3-dioxolane (DOL) and dimethyl ether (DME) at a volume ratio of 1:1 were used as the electrolyte, purchased from Fosai New Material Co., Ltd (Suzhou). The flexible freestanding NCNF2-900 coated celgard@ separator film was prepared by coating NCNF2-900 slurry composed of NFHCS and PVDF with the weight ratio of 8:2 on the separator. After drying at 60℃ for 10h under vacuum, a large piece of flexible NFHCS coated celgard separator was obtained. The mass loading of NCNF2-900 in the interlayer is around 0.3 mg cm^{-2} [4].

Galvanostatic charge/discharge tests were conducted to evaluate the electrochemical capacity and cycle stability of the electrodes on the basis of the active

sulfur at current densities of 0.2 C, 0.5 C, 1 C, 2 C, 3 C, 5 C (1 C = 1675 mA h g^{-1}) from 1.5 to 3.0 V using a LANHE instrument (Wuhan Land electronics Co., Ltd China). CV data were recorded on a CHI660e electrochemical workstation (Shanghai Chenhua) between 1.6 and 2.8 V to characterize the redox behavior and the kinetic reversibility of the cell. The ac impedance was measured with fresh cells at the open circuit potential. This was also carried out using a CHI 660e electrochemical workstation. The ac amplitude was 5 mV and the frequency ranged from 100 kHz to 0.01 Hz.

Adsoption of Lithium Polysulfide

Lithium polysulfide (Li_2S_6) was synthesized according to the literature [1]. The adsorption ability of the NCNF2-700, NCNF2-750, NCNF2-800, NCNF2-900 and NCNF2-1000 on lithium polysulfide was investigated by UV-Vis spectroscopy (UV1800 spectrophotometer Shimadzu). Typically, 50 mg of each carbon host was soaked in 5 mL of Li_2S_6 solution (5 mM), and the mixture was stirred for 30 min.

Materials characterization

The content of sulfur was tested using a TG/DTA thermogravimetric analyzer (Diamond PE) under an N_2 atmosphere at a heating rate of 10 °C min^{-1} from room temperature to 600 °C, with a flow rate of 80 mL min^{-1}. SEM images were obtained with a Nova NanoSEM 200 scanning electron microscope (FEI, Inc.). TEM, HRTEM images were achieved with a JEOL2100 instrument. Powder XRD was recorded on a Bruker D8 Advance X-ray diffractometer using CuKa radiation (λ= 0.15418 nm) at a scanning rate of 4ºmin^{-1} in the 2θ range from 10º to 80º. X-ray photoelectron spectroscopy (XPS) measurements were conducted with an ultrahigh vacuum setup, equipped with a monochromatic Al Ka X-ray source and a high resolution Thermo ESCALAB 250 analyzer. Raman spectra were collected on a Labram-010 microscopic confocal Raman spectrometer with a 633 nm laser excitation. Specific surface area, pore volume and pore size distribution were determined by the BET method on a Micromeritics ASAP 2020 instrument.

Table S1 Specific surface area and pore volume of NCNF1-800, NCNF2-800 and NCNF3-800 evaluated by the Brunauer-Emmett-Teller (BET) and density functional theory (DFT) method, respectively.

Sample Name	SSA (m^2/g)	Pore Volume (cm^3/g)
NCNF1-800	686	1.60
NCNF2-800	873	1.69
NCNF3-800	482	1.22

Table S2 The content of C, N and O evaluated by the XPS spectrum in Fig. 2b.

Sample Name	C	N	O
NCNF1-800	90.48%	4.51%	5.01%
NCNF2-800	88.26%	7.82%	3.92%
NCNF3-800	88.08%	6.94%	4.98%

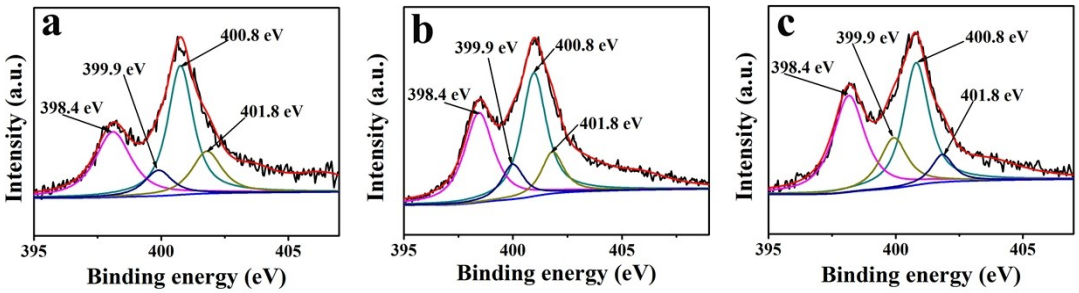

Fig. S1 The high resolution XPS of N1s peaks for NCNF1-800, NCNF2-800 and NCNF3-800.

Table S3 The content of different nitrogen species for NCNF1-800, NCNF2-800 and NCNF3-800.

Sample Name	pyridinic-N	pyrrolic-N	graphitic -N	oxygen-N
NCNF1-800	1.40%	0.42%	1.95%	0.74%
NCNF2-800	2.79%	0.82%	3.23%	1.19%
NCNF3-800	2.61%	1.18%	2.65%	0.50%

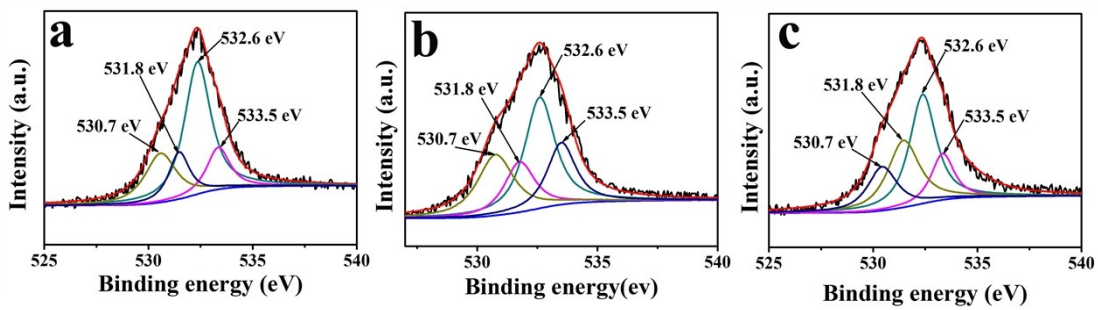

Fig. S2 The high resolution XPS of O1s peaks for NCNF1-800, NCNF2-800 and NCNF3-800.

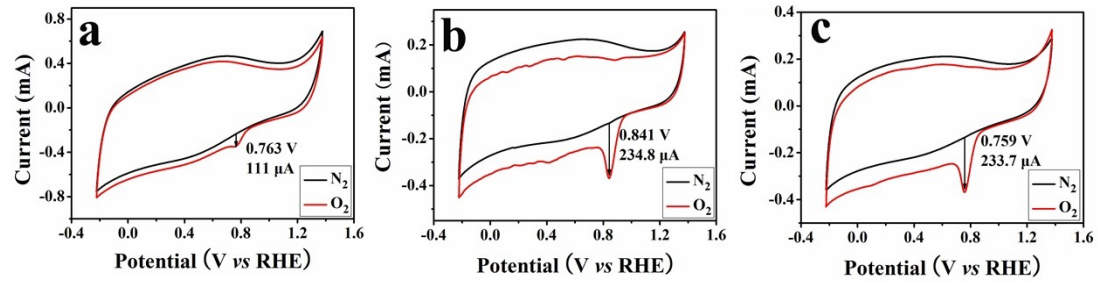

Fig. S3 CVs recorded for the NCNF1-800 (a), NCNF2-800 (b) and NCNF3-800 (c) electrodes

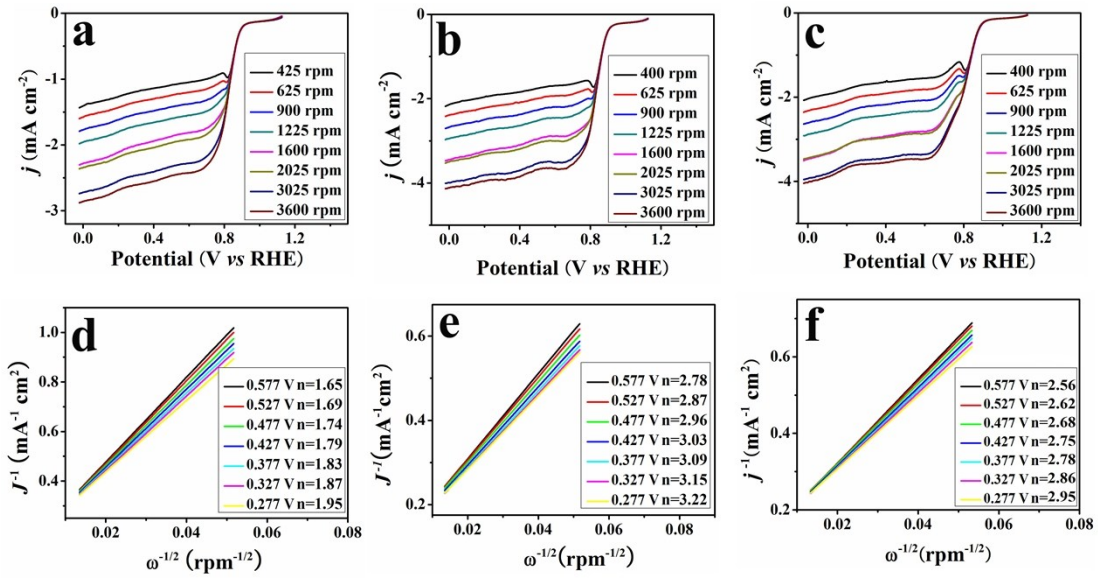

Fig. S4 RDE recorded for the NCNF1-800 (a), NCNF2-800 (b) and NCNF3-800 (c) electrodes at different rotation rates; Electron-transfer numbers as a function of the over-potential of NCNF1-800 (d), NCNF2-800 (e) and NCNF3-800 (f) electrodes at different potentials. Koutecky-Levich plot of J^{-1} *vs* $\omega^{-1/2}$ at different electrode potentials. The experimental data were obtained from (a-c); the lines are linear regressions.

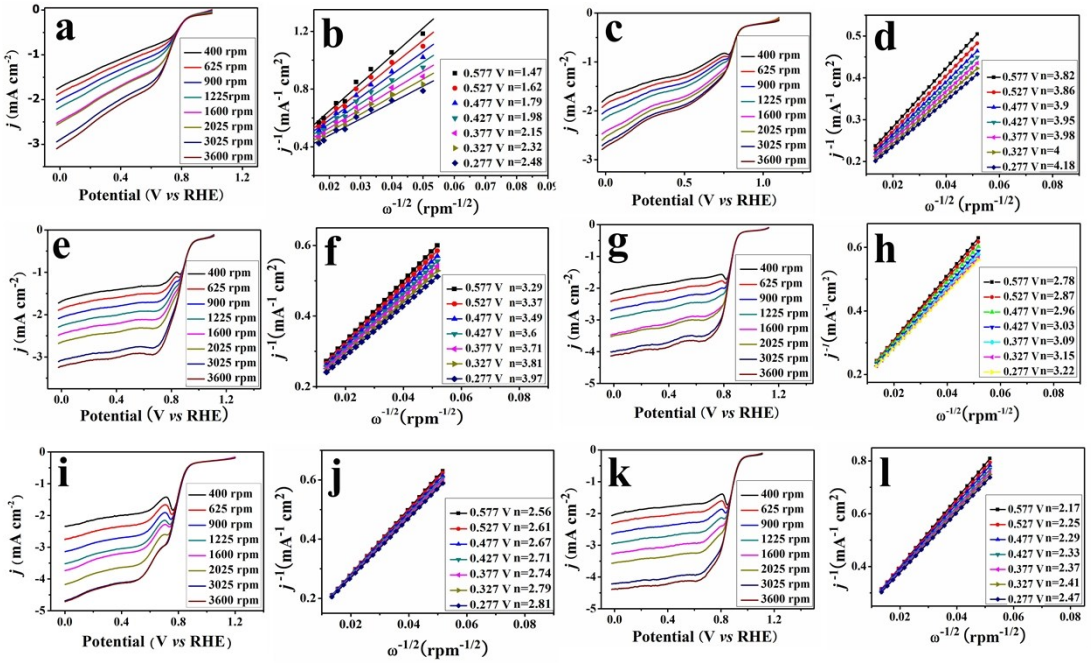

Fig. S5 LSV curves of NCNF2-600 (a), NCNF2-700(c), NCNF2-750(e), NCNF2-800(g), NCNF2-900(i) and NCNF2-1000(k) respectively at different rotation rates with a scan rate of 10 mV s^{-1}; Electron-transfer numbers as a function of the over-potential of NCNF2-600(b), NCNF2-700(d), NCNF2-750(f), NCNF2-800(h), NCNF2-900(j) and NCNF2-1000(l) electrodes at different potentials. Koutecky-Levich plot of J^{-1} *vs* $\omega^{-1/2}$ at different electrode potentials.

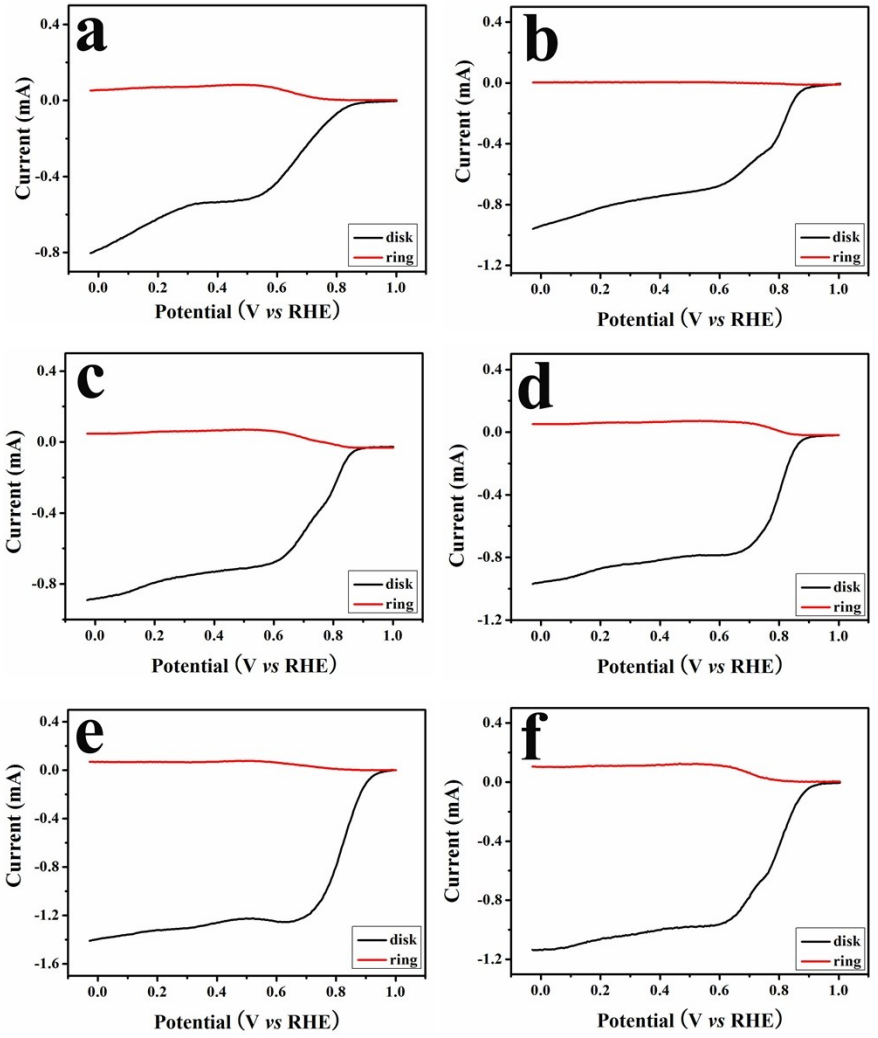

Fig. S6 Rotating ring disk electrode (RRDE) Linear sweep voltammograms of NCNF2-600, NCNF2-700, NCNF2-750, NCNF2-800, NCNF2-900 and NCNF2-1000.

Table S4 Specific surface area and pore volume of NCNF2-600, NCNF2-700, NCNF2-750, NCNF2-800, NCNF2-900 and NCNF2-1000 evaluated by the Brunauer-Emmett-Teller (BET) and density functional theory (DFT) method, respectively.

Sample Name	**SSA** ($m^2\ g^{-1}$)	**Pore Volume** ($cm^3\ g^{-1}$)	**Micropore Volume** ($cm^3\ g^{-1}$)	**MesoporeVolume** ($cm^3\ g^{-1}$)
NCNF2-600	721	1.30	0.27	1.03
NCNF2-700	775	1.33	0.27	1.06
NCNF2-750	845	1.47	0.28	1.19
NCNF2-800	873	1.69	0.30	1.39
NCNF2-900	907	1.85	0.31	1.54
NCNF2-1000	642	1.47	0.21	1.26

Table S5 The content of C, N and O evaluated by the XPS spectrum in Fig. 8.

Sample Name	C	N	O
NCNF2-600	84.91%	8.63%	6.45%
NCNF2-700	86.36%	8.72%	4.92%
NCNF2-750	87.18%	8.44%	4.38%
NCNF2-800	88.26%	7.82%	3.92%
NCNF2-900	90.92%	5.2%	3.88%
NCNF2-1000	91.77%	3.6%	4.63%

Table S6 The content of different nitrogen species for NCNF2-600, NCNF2-700, NCNF2-750, NCNF2-800, NCNF2-900 and NCNF2-1000.

Sample Name	Total N	pyridinic-N	pyrrolic-N	graphitic-N	oxygen-N
NCNF2-600	8.63%	3.88%	0.84%	3.69%	0.22%
NCNF2-700	8.72%	3.48%	0.93%	3.43%	0.88%
NCNF2-750	8.44%	2.59%	0.57%	4.76%	0.52%
NCNF2-800	7.82%	2.79%	0.82%	3.23%	1.19%
NCNF2-900	5.20%	1.76%	0.49%	2.35%	0.60%
NCNF2-1000	3.60%	0.60%	0.30%	1.86%	0.84%

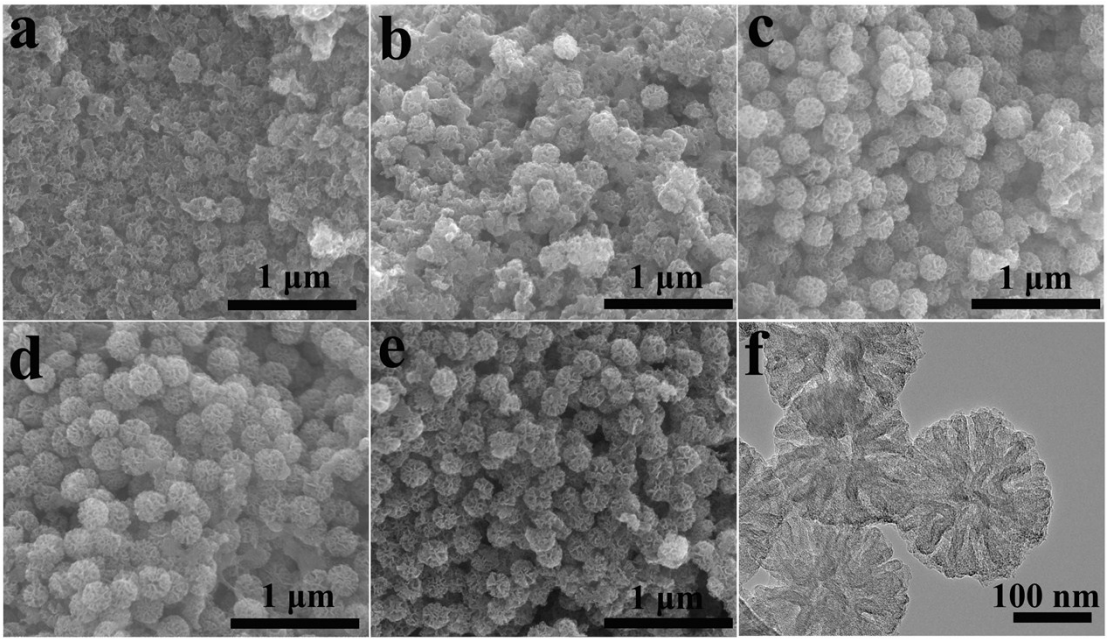

Fig. S7 SEM images of the NCNF2-700/S80%(a), NCNF2-750/S80%(b), NCNF2-800/S80%(c), NCNF2-900/S80%(d) and NCNF2-1000/S80%(e), respectively; TEM image of NCNF2-900/S 80%(f).

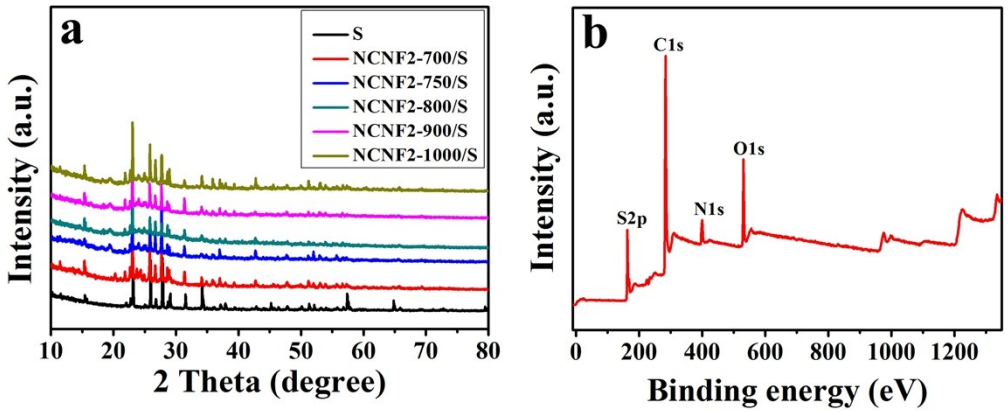

Fig. S8 (a) XRD patterns of the NCNF2-700/S80%, NCNF2-750/S80%, NCNF2-800/S80%, NCNF2-900/S80%and NCNF2-1000/S80%; (b) the wide XPS survey of NCNF2-900/S80%.

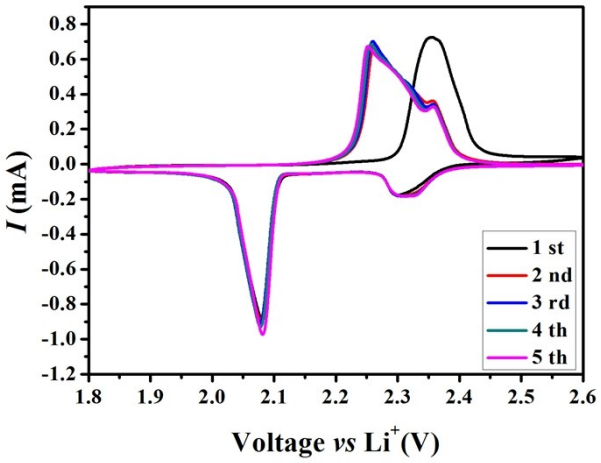

Fig. S9 Cyclic voltammograms of NCNF2-900/S80%/Li cell at a scan rate of 0.02 mV s^{-1}.

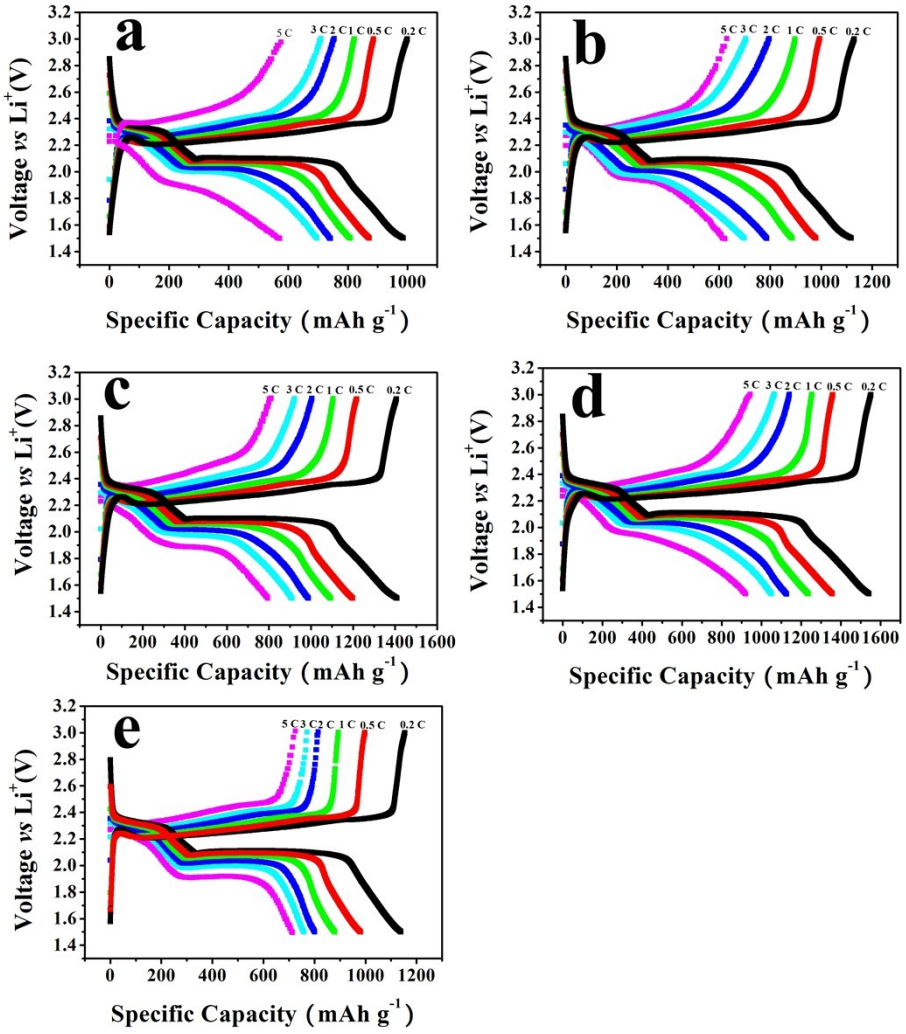

Fig. S10 The discharge-charge profiles of NCNF2-700/S80%, NCNF2-750/S80%, NCNF2-800/S 80%, NCNF2-900/S 80%and NCNF2-1000/S 80%/Li cells, respectively.

Table S7 The rate performance of NCNF2-700/S80%, NCNF2-750/S80%, NCNF2-800/S80%, NCNF2-900/S80% and NCNF2-1000/S80%/Li cells, respectively.

Sample	0.2 C (mAh g^{-1})	0.5 C (mAh g^{-1})	1 C (mAh g^{-1})	2 C (mAh g^{-1})	3 C (mAh g^{-1})	5 C (mAh g^{-1})	0.2 C (mAh g^{-1})
NCNF2-700/S80%	987	873	808	742	696	571	877
NCNF2-750/S80%	1118	980	887	788	699	624	1008
NCNF2-800/S80%	1410	1198	1094	988	911	795	1242
NCNF2-900/S80%	1633	1358	1238	1127	1051	921	1377
NCNF2-1000/S80%	1139	981	880	801	759	714	1002

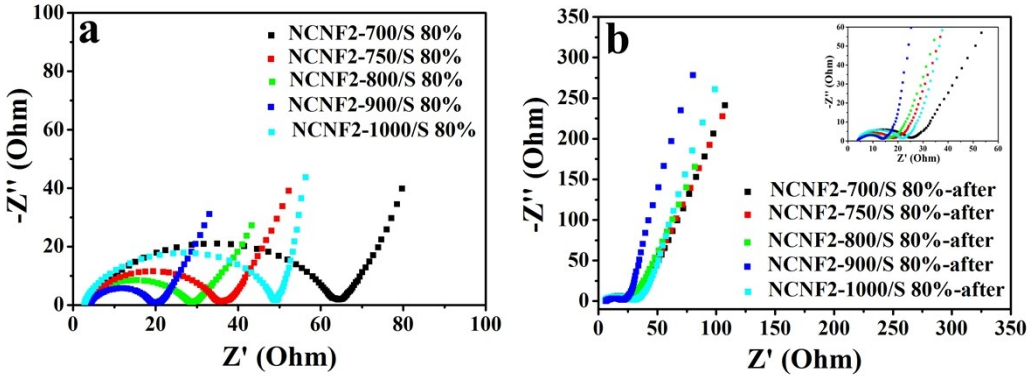

Fig. S11 Nyquist plots of before (a) and after 500 cycles (b) of battery testing of the NCNF2-700/S80%, NCNF2-750/S80%, NCNF2-800/S80%, NCNF2-900/S80% and NCNF2-1000/S80%/Li cells.

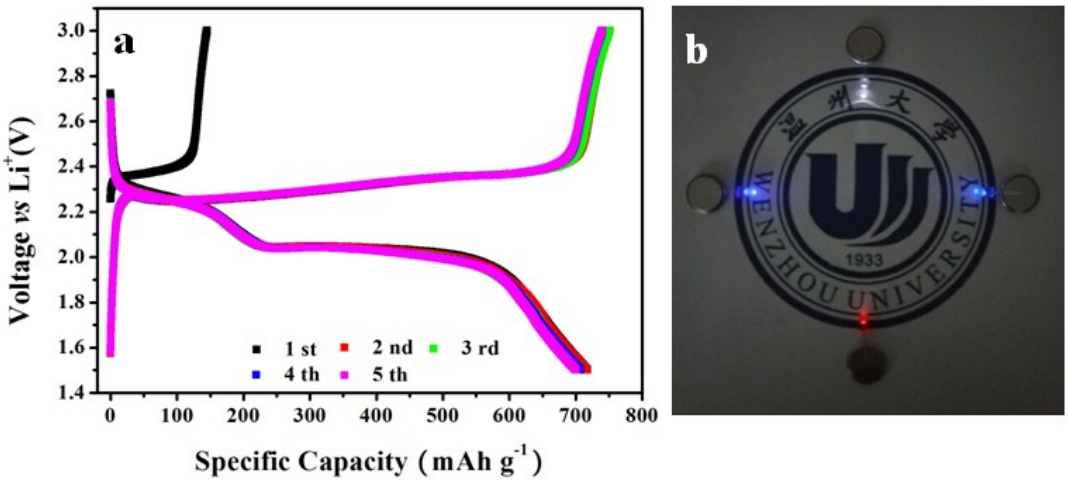

Fig. S12 The discharge-charge profiles at 0.2 C and the photograph lighting up the indicators of LED modules for the cells with NCNF2-900/S80% cathodes with a high sulfur loading of 2.5 mg cm^{-2} after 500 cycles placed for about 300 days.

Table S8 A comparison of cycling performance between this work and some other Li-S cells with loading high sulfur area density reported in previous literature.

Cathode materials	Sulfur Loading area density (mg cm^{-2})	Cycling performance	Capacity Decay rate per cycle	Refs.
G/CNT/S80/IKB	4.7	0.2C, 90 cycles, 900~700 mAh g^{-1}	0.25	5
TiC@G	3.5	0.2C, 100 cycles, 1032~670 mAh g^{-1}	0.35%	6
LDH@NG	4.3	1.0 mA cm^{-2}, 100cycles 1078-800 mAh g^{-1}	0.25%	7
LDH/S	3.0	0.1C, 100 cycles, 1014~653 mAh g^{-1}; 0.5C, 100 cycles, 747~491 mAh g^{-1}	0.35% 0.34%	8
CNT-nest-85%S	3.0	0.1C, 80 cycles, 937~800 mAh g^{-1}	0.14%	9
HCG-HPG/S	5	0.34 A g^{-1} (~1.7 mA cm^{-2}), 400 cycles, 7.5~4.2 mAh cm^{-2}	0.11%	10
PCNTs-S@Gra/DT	4.4	1.17mA cm^{-2} (0.2C), 200 cycles, 1253~984 mAh g^{-1}; 1.10mA cm^{-2} (0.15C), 200cycles, 1018~683 mAh g^{-1}	0.11% 0.16%	11
NCNF/S	4.5	3.77 mA cm^{-2} (0.5 C), 200 cycles, 758~654 mAh g^{-1}	0.07%	-

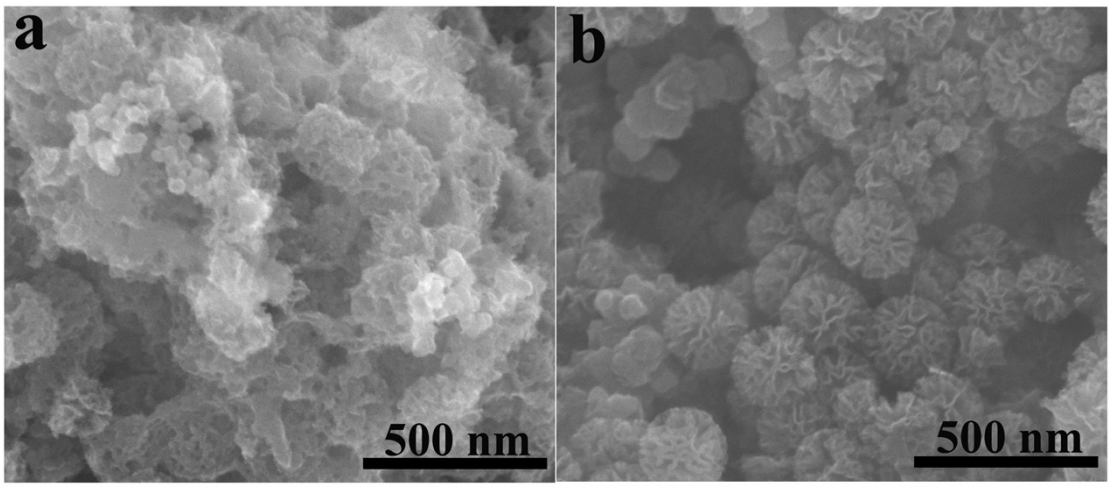

Fig. S13 SEM images of the rNCNF2-700(a) and rNCNF2-900(b).

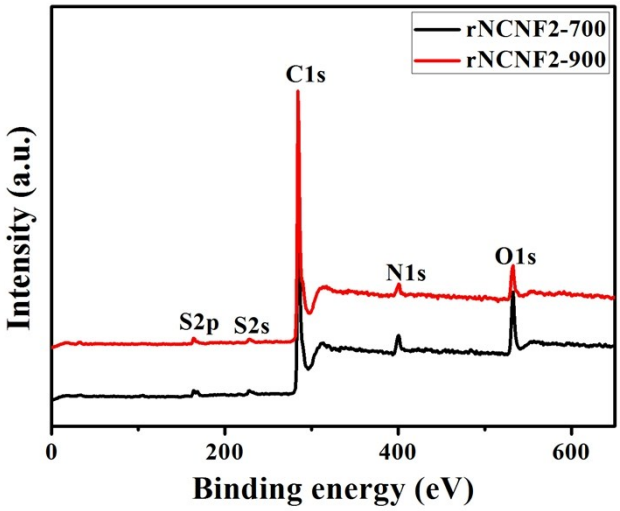

Fig. S14 The wide XPS survey of rNCNF2-700 and rNCNF2-900.

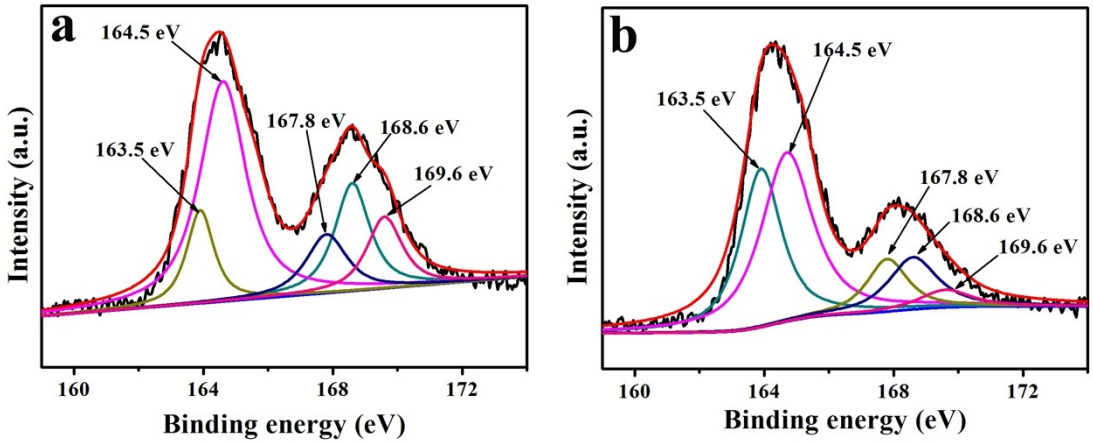

Fig. S15 The high resolution XPS of S2p peaks for the rNCNF2-700(a) and rNCNF2-900(b).

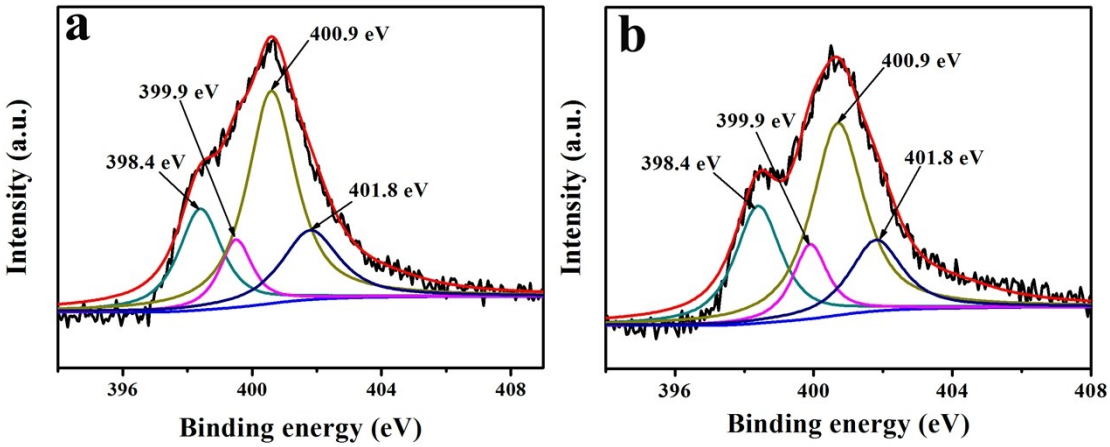

Fig. S16 The high resolution XPS of N1s peaks for the rNCNF2-700(a) and rNCNF2-900(b).

Table S9 The content of C, N and O evaluated by the XPS spectra in Fig. S13.

Sample Name	C	N	O	S
rNCNF2-700	85.12%	5.96%	7.04%	1.88%
rNCNF2-900	91.07%	3.97%	3.32%	1.64%

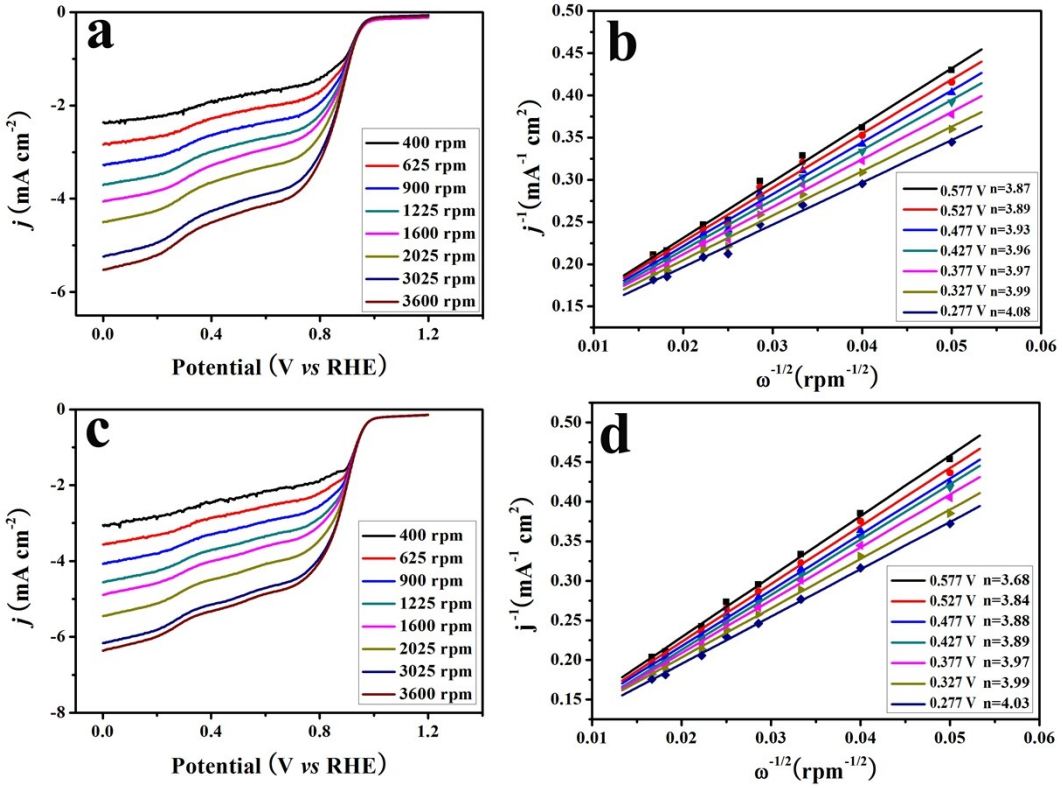

Fig. S17 LSV curves of rNCNF2-700(a) and rNCNF2-900(c) at different rotation rates with a scan rate of 10 mV s^{-1}; Electron-transfer numbers as a function of the over-potential of rNCNF2-700(b) and rNCNF2-900(d) electrodes at different potentials. Koutecky-Levich plot of J^{-1} *vs* $\omega^{-1/2}$ at different electrode potentials.

Table S 10 A comparison on the onset potential, half-wave potential and kinetic current density of NCNF2-700, NCNF2-900, rNCNF2-700, rNCNF2-900 and Pt/C catalysts

Sample Name	NCNF2-700	NCNF2-900	rNCNF2-700	rNCNF2-900	Pt/C
Onset potential	0.86	0.95	0.97	0.10	0.99
Half-wave potentials	0.79	0.84	0.90	0.91	0.86
Current density	7.80	9.38	10.34	13.26	8.61

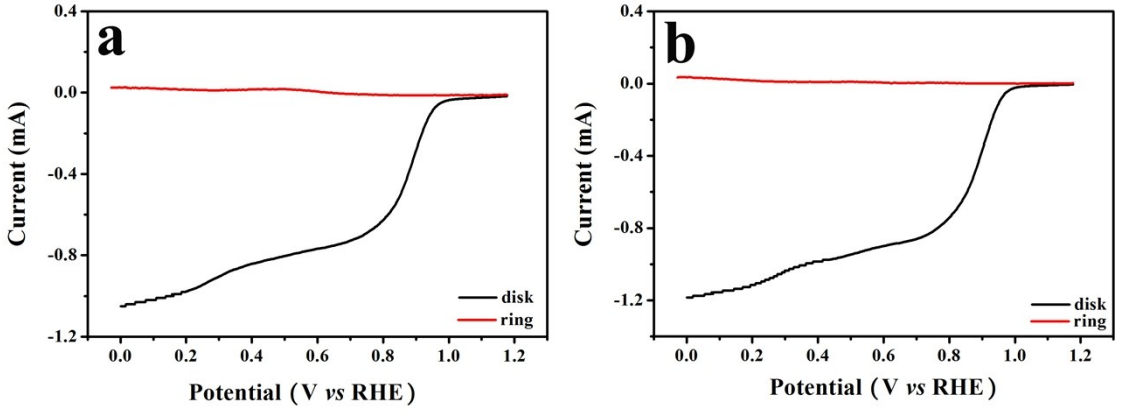

Fig. S18 Rotating ring disk electrode (RRDE) Linear sweep voltammograms of rNCNF2-700 and rNCNF2-900.

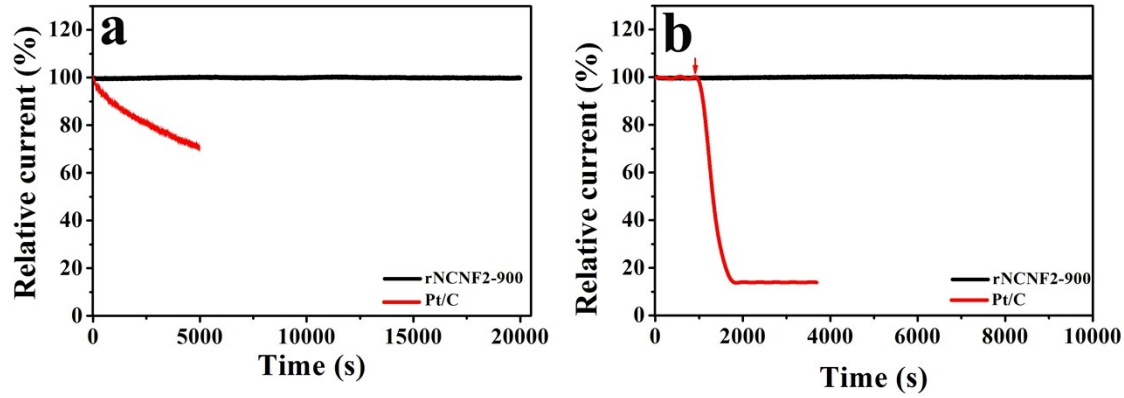

Fig. S19 (a) Chronoamperometric responses of NCNF2-900 and Pt/C modified GC electrodes; (b) with 3 M methanol added at around 1000 s and (b) at 0.7 V (*vs* RHE) in an O_2-saturated 0.1 M KOH solution

Table S11 A comparison of comprehensive performance between this work and some other Li-S cells based on the carbon materials reported in previous literature.

Cathode materials (sulfur host)	Sulfur Loading	Capacity(calculate based on the sulfur)	stability (decay rate per cycle, cycles)	Refs.
Tailoring Porosity in Carbon Nanospheres	70%	1015 0.2 C 920 0.5C 875 1C	0.1% per cycle for 100 cycles at 1C	12
Hierarchical Porous Carbon nanosheets	74%	1370 0.5C 1200 1C 860 5C	0.25% decay for 100 cycles at 1 C	13
Hierarchical Vine-Tree-Like Carbon Nanotube Architectures	60%	1418 0.5C (initial) 997 3C 630 4C	0.08% decay for 450 cycles at 1 C	14

Polydopamine-Coated, Nitrogen-Doped, Hollow Carbon	55%	1070 0.2C 740 0.6C	0.1% decay per cycle for 150 cycles at 0.2 C	15
Graphene/Sulfur Hybrid Nanosheets	68%	1200 0.2 C 700 2C 400 5C	0.5% decay for 70 cycles at 0.5 C	16
ultrahigh-surface-area hollow carbon nanospheres	67%	1240 0.2C 1026 0.5C 965 1 C 655 2C	0.07% decay per cycle for 500 cycles at 0.5C	17
Nitrogen-Doped Hollow Carbon Nanospheres	85%	1139 0.2C 920 0.5C 720 1C 250 2C	0.12% decay for 200 cycles at 0.2 C	18
Hierarchical carbon nanocages	79.8%	1214 0.2 A g^{-1} 580 3 A g^{-1}	0.16 % decay for 300 cycles at 1 A g^{-1}	19
h-CNT/S/ZrO_2 composite cathode	45.2%	4c 1000 10c 850	0.11% decay per cycle for 200 cycles at 0.5 C	20
Nitrogen and Sulfur Dual-Doped Carbon	70%	1370 0.05C 1280 0.2C 1135 0.5C 830 2C	0.052% decay per cycle for 1000 cycles at 0.5 C	21
Multichannel Carbon Nanofiber	80%	1351 at 0.2 C 847 at 5C	0.07% decay per cycle for 300 cycles at 0.2C	22
Three-dimensional porous carbon	90%	1382 0.5C 1242 1C 1115 2 C	0.039% decay for 1000 cycles at 2 C	23
Graphitic carbon nanocage	77%	1024 0.5C 900 1C 875 2C 765 5C	0.0215% for 1000 cycles decay at 1 C	24
Incorporating Sulfur Inside the Pores of Carbons by An Electrolysis Approach	70%	1068 0.5C 869 1 C 725 2C 652 4C	0.08 % decay per cycle for 500 cycles at 0.5 C	25
Highly Crumpled Nitrogen-Doped Graphene Sheets	80%	1100 0.2C 1000 0.5C 950 1C	0.08% decay per cycle for 300 cycles at 1.17 mA cm^{-2}	4
Si/SiO_2@Hierarchical Porous Carbon Spheres	69.6 %	1230 0.1C 1002 0.5C 907 1C 614 2C	0.063% decay per cycle for 500 cycles at 2 C	26
Mesoporous Carbon	60%	753 1C	0.093 % decay per	27

Nanotube Network		701 2C 655 5C	cycle for 100 cycles	
N-Doped Hollow Porous Carbon Bowls	70%;	1065 0.5C 882 1C 785 2C 600 3C 535 4C	0.053% decay per cycle for 400 cycles at 1 C	28
Hierarchical Porous Graphene	68%	887 0.1 C 656 5C	0.11% decay per cycle for 150 cycles at 0.5 C	29
S@Co–N-GC	70%	925 0.5 C 795 1C 685 2C 565 5C	0.057% decay per cycle for 500 cycles at 1 C	30
3D Graphene Nanosheet@Carbon Nanotube Matrix	76.4%	695.3 0.5C 598.0 1C 408.6 2C (based composites)	0.09% decay per cycle for 500 cycles at 1 C	31
Honeycomb-like Ordered Mesoporous Carbon Nanosheets	70%	840 0.5 C 753 1C 580 2C	0.081% decay per cycle for 500 cycles at 0.5 C	32
N- doped carbon nanoflower	80%	1358 0.5 C 1238 1C 1127 2C 921 5C	0.07% decay per cycle for 500 cycles at 1 C	This work

References:

1. N. M. Markvić, H. A. Gasteiger and P. N. Ross, *J. Phys. Chem*., 1996, **100**, 6715-6721
2. Wu J, Jin C, Z. R. Yang, J. H. Tian and R. Z. yang, *Carbon*, 2015, **82**, 562-571
3. Y. Hu, J. O. Jensen, W. Zhang, L. N. Cleemann, W. Xing, N. J. Bjerrum and Q. F. Li, *Angew. Chem., Int. Ed*., 2014, **53**, 3675-3679
4. J. X. Song, Z. X. Yu, M. L. Gordin and D. H. Wang, *Nano Lett.*, 2016, **16**, 864-870.
5. D. P. Lv, J. M. Zheng, Q. Y. Li, X. Xie, S. Ferrara, Z. M. Nie, L. B. Mehdi, N. D. Browning, J. G. Zhang, G. L. Graff, J. Liu and J. Xiao, *Adv. Energy Mater*., 2015, **5**, 1402290
6. H. J. Peng, G. Zhang, X. Chen, Z. W. Zhang, W. T. Xu, J. Q. Huang, Q. Zhang, *Angew. Chem. Int. Ed*., 2016, **55**, 13184-13189.
7. H. J. Peng, Z. W. Zhang, J. Q. Huang, G. Zhang, J. Xie, W. T. Xu, J. L. Shi, X. Chen, X. B. Cheng, Q. Zhang, *Adv. Mater.*, 2016, **28**, 9551-9558.
8. J. T. Zhang, H. Hu, L. Zhen and X. W. Lou, *Angew. Chem. Int. Ed*., 2016, **55**, 3982-3986.
9. A. Guo, Y. L.Dai, W. F. Mao, H. Zhao, Y. B. Fu, X. Y. Song, Y. F. En, V. S. Battaglia, V. Srinivasan and G. Liu, *Nano Lett*., 2016, **16**, 5365-5372.
10. R. P. Fang, S. Y. Zhao, S. F. Pei, X. T. Qian, P. X. Hou, H. M. Cheng, C. Liu and F. Li, *ACS Nano*, 2016, **10**, 8676-8682.

11. W. X. Hua, Z. Yang, H. G. Nie, Z. Y. Li, J. Z. Yang, Z. Q. Guo, C. P. Ruan, X. A. Chen and S. M. Huang, *ACS Nano*, 2017, **11**, 2209-2218.
12. G. He, S. Evers, X. Liang, M. Cuisinier, A. Garsuch and L. F. Nazar, *ACS Nano*, 2013, **7**, 10920-10930.
13. X. A. Chen, Z. B. Xiao, X. T. Ning, Z. Liu, Z. Yang, C. Zou, S. Wang, X. H. Chen, Y. Chen and S. M. Huang, *Adv. Energy Mater*., 2014, **4**, 1301988.
14. M. Q. Zhao, H. J. Peng, G. L. Tian, Q. Zhang, J. Q Huang, X. B. Cheng, C. Tang and F. Wei, *Adv. Mater*., 2014, **26**, 7051-7058
15. W. D. Zhou, X. C. Xiao, M. Cai and L. Yang, *Nano Lett*., 2014, **14**, 5250-5256.
16. L. F. Fei, X. G. Li, W. T. Bi, Z. W. Zhuo, W. F. Wei, L. Sun, W. Lu, X. J. Wu, K. Y. Xie, C. Z. Wu, H. L. W. Chan and Y. Wang, *Adv. Mater*., 2015, **27**, 5936-5942.
17. F. Xu, Z. W. Tang, S. Q. Huang, L. Y. Chen, Y. R. Liang, W. C. Mai, H. Zhong, R. W. Fu and D. C. Wu, *Nat. Commun.*, 2015, **6**, 7221.
18. W. D. Zhou, C. M. Wang, Q. L. Zhang, H. D. Abruña, Y. He, J. W. Wang, S. X. Mao and X. C. Xiao, *Adv. Energy Mater*., 2015, **5**, 1401752.
19. Z. Y. Lyu, D. Xu, L. J. Yang, R. C. Che, R. Feng, J. Zhao, Y. Li, Q. Wu, X. Z. Wang and Z. Hu. *Nano Energy*, 2015, **12**, 657-665.
20. Y. Zhou, C. G. Zhou, Q. Y. Li, C. J. Yan, B. Han , K. S. Xia, Q. Gao and J. P. Wu, *Adv. Mater.*, 2015, 27, 3774-3781.
21. Q. Pang, J. T. Tang, H. Huang, X. Liang, C. Hart, K. C. Tam and L. F. Nazar, *Adv. Mater.*, 2015, **27**, 6021-6028.
22. J. S. Lee, W. Kim, J. Jang and A. Manthiram, *Adv. Energy Mater*., 2016, 1601943.
23. G. X. Li, J. H. Sun, W. P. Hou, S. D. Jiang, Y. Huang and J. X. Geng, *Nat. Commun*., 2016, **7**, 10601.
24. J. Zhang, C. P. Yang, Y. X. Yin, L. J. Wan and Y. G. Guo, *Adv. Mater*., 2016, **28**, 9539-9544.
25. B. He, W. C. Li, C. Yang, S. Q.Wang and A. H. Lu, *ACS Nano*, 2016, **10**, 1633-1639.
26. S. Rehman, S. J. Guo and Y. L. Hou, *Adv. Mater*., 2016, **28**, 3167-3172.
27. L. Sun, D. T. Wang, Y. F. Luo, K. Wang, W. B. Kong, Y. Wu, L. Zhang, K. L. Jiang, Q. Q. Li, Y. H. Zhang, J. P. Wang and S. S. Fan. *ACS Nano*, 2016, **10**, 1300-1308.
28. F. Pei, T. H. An, J. Zang, X. J. Zhao, X. L. Fang, M. S. Zheng, Q. F. Dong and N. F. Zheng, *Adv. Energy Mater*., 2016, 1502539.
29. C. Tang, B. Q. Li, Q. Zhang, L. Zhu, H. F. Wang, J. L. Shi and F. Wei, *Adv. Funct. Mater*., 2016, **26**, 577-585.
30. Y. J. Li, J. M. Fan, M. S.Zheng and Q. F. Dong, *Energy Environ. Sci*., 2016, **9**, 1998-2004.
31. Z. Zhang, L. L. Kong, S. Liu, G. R. Li and X. P. Gao, *Adv. Energy Mater*., 2017, 1602543.
32. S. K. Park, J. Lee, T. Hwang, B. Jang and Y. Piao.*ACS Appl. Mater. & Interfaces*, 2017, **9**, 2430-2438.